Impact of Perlator on the cooling liquid flow and hottest point temperature of superconducting windings in HTS transformer

Mahdi Mahamed [a], Mohammad Yazdani-Asrami [b,*], Vahid Behjat [c], Akbar Yazdani [d], Mojtaba Sharifzadeh [e]

[a] Department of Electrical Engineering, Azarbaijan Shahid Madani University, Tabriz, Iran
[b] Propulsion, Electrification & Superconductivity Group, James Watt School of Engineering, University of Glasgow, Glasgow, UK
[c] Department of Applied Sciences, University of Quebec at Chicoutimi, Chicoutimi, Canada
[d] Thermal Power Plant Research Center, Tabriz, Iran
[e] Fondazione Bruno Kessler, Trento, Italy

ARTICLE INFO

ABSTRACT

The generated heat by the superconducting windings and the other parts such as current leads in transformer increases the hottest point temperature (HPT) and causes the high temperature superconducting (HTS) windings to quench. Due to the properties of superconducting windings, reducing the HPT is of critical importance for the stable operation of the HTS transformer. The cooling system of HTS transformers, not only provides the cryogenic temperature for the proper operation of the superconductors but also is responsible for dissipating the generated heat by the windings. In this paper, the effect of the angle of inlet pipes in cooling system was investigated. This was a simple and effective solution which increases the heat transfer in liquid nitrogen. It was shown that inlet angle has a significant effect on the flow turbulence and the windings temperature. The Perlator is used as a lattice sheet which is installed inside the inlet valve and increases the turbulence of inlet flow of liquid nitrogen to increase heat transfer and reduce HPT. The thermal analysis is obtained by finite element method using ANSYS Fluent software. The influence of changing the inlet pipe angle and different structure of Perlator on heat transfer was investigated.

1. Introduction

High temperature superconducting (HTS) transformers have various advantages compared to conventional transformers such as their reduced the size, weight, losses as well as increased efficiency (>99%) [1–7]. Furthermore, due to the use of liquid nitrogen (LN$_2$) instead of oil, the risks and environmental damages are reduced [8].

The hottest point temperature (HPT) is the most sensitive point in HTS transformers for probable quenches. During the design procedure of HTS transformers, the HPT point of winding in terms of stability and reliability of the transformer is the most important. Moreover, the windings temperature reduction in the transformer design has several advantages, including the power reduction of the cooling system, which increases the efficiency of the transformer [9] and increasing the critical current of the windings, which reduces the AC loss [10]. There are two major solutions for design engineers of HTS transformers to reduce the risk of HPT at the windings. The first solution is to increase the rate of heat transfer to the outside of the cryogenic environment and the second solution is to decrease the AC loss of the HTS transformer.

Different solutions to reduce the HPT of the HTS transformer are presented [7,11–13]. These solutions mostly use flux diverter which reduces the radial and axial leakage magnetic fields in the HTS transformer. The second solution is heat transfer increase in which the velocity, flow direction, and turbulence of cryogenic fluid are three major factors to increase heat transfer. Between these factors, increasing the turbulence of the LN$_2$, in addition to reduction of the HPT, causes the average temperature of windings to be reduced. In [14], the number and location of inlet and outlet pipes are investigated and the optimal flow velocity of the LN$_2$ to reduce the hottest point temperature was investigated. In [15], the layout of inlet pipe on the bottom of cryostat was investigated and concluded that the inlet valve should be located near the hottest point of windings. However, in these papers, the effect of inlet pipe angle and LN$_2$ turbulence on reducing the temperature of the hottest point was not investigated. In [16] the efficiency of turbulence rate on heat transfer of LN$_2$ was studied and showed that increasing turbulence increases the heat

transfer rate. In [17], heat transfer in porous plates was studied and showed that heat transfer in these plates increases by 10–20%. In [18], the importance of heat transfer in HTS transformers was further discussed. AC loss is a major cause of heat generation in the HTS windings of transformers which must be considered in thermal analysis. For simple and integrated geometries (such as solenoid windings and transformer core) analytical methods are presented in [19] to calculate the AC loss values. In order to calculate AC loss in complex geometries researchers widely used FEMs. To calculate AC loss of HTS tapes and HTS coils, the H-formulation method are achieved which shows good agreement with experimental tests [20,21]. In [22], a 120 kVA, 6 kV/0.4 kV, single-phase HTS transformer operating at 77 K, was designed but its cooling system was not considered. Additionally, magnetic field distribution and AC loss values in double pancake coils were reported. Due to the high density of perpendicular field in HTS transformers, the AC loss is relatively high. On other hand, the double-pancake is easy to quench in the case that AC loss produces a large amount of heat [14]. The solution to this problem is studied in this presented paper.

In this paper, a cryostat system for 120 kVA, 6 kV/0.4 kV, single-phase HTS transformer is designed to increase the turbulence of LN$_2$ which will lead to a significant improvement in heat transfer performance and will reduce the HPT of windings. The specification of this HTS transformer and its superconducting tapes are tabulated in Table 1. Installing a Perlator and finding an orthogonal angle to the natural flow of the fluid for the inlet flow are two simple and inexpensive ways to increase turbulence. For this purpose, the temperature distribution in superconducting windings and fluid movement inside the cryostat for different inlet valve angles were analyzed after adding a Perlator. Various structures of Perlators were considered and studied to select the most suitable structure. Finally, the rate of turbulence, the flow velocity, the heat transfer rate and the temperature distribution in different parts of HTS transformer, by different inlet valve angles and different Perlator structure, were presented.

2. The cryostat model of an HTS transformer with Perlator

2.1. Cryostat specification

The schematic of the HTS transformer including windings, cryostat, inlet, outlet valves, and other parts are shown in Fig. 1.

As shown in this figure, inlet and outlet valves that are connected to cryostat pump are on the top and bottom of the cryostat, respectively. It should be mentioned that the double pancake and solenoid windings consist of Bi2223 tapes are used for the low and high voltage windings, respectively. LN$_2$ at a pressure of 1 atmosphere and temperature of 77 K and at a velocity rate of 1.3 m/s is pumped by means of an electro-pump into the cryostat to stabilize the temperature of the
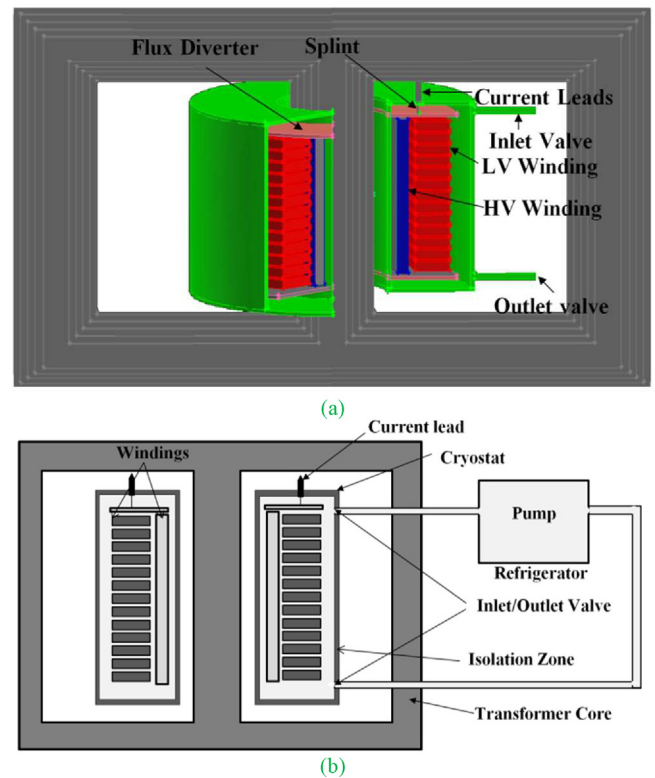

(a)

(b)

Fig. 1. Structure of cryostat system in the understudied HTS transformer.

HTS windings. Afterwards, the warmed-up coolant is transferred by the outlet valve to the cooling system. The cryostat walls are made out of Fiber-reinforced polymer (FRP) materials. Other specifications of the cryostat are shown in Table 2.

In Fig. 2, the distribution of LN$_2$ flow is shown. The blue arrows and the red arrows show the cold and hot LN$_2$ flow directions, respectively. As shown in Fig. 2 the cold LN$_2$ partials by collision to windings surface, their temperature rises and move to upside.

2.2. Numerical calculation

The purpose of this study is to optimize the design of the inlet valve angle θ to reach a minimum HPT in the transformer winding.

The natural movement of LN$_2$ inside the cryostat is vital for determining and designing the angle. In this case, if the flow direction of the fluid near the inlet valve (turbulence effective zone) is perpendicular to the angle of the inlet valve, it would create higher turbulence and thus, heat transfer would be improved. For this purpose, the LN$_2$ movement inside the cryostat for different angles of the inlet valve needs to be analyzed to find the optimum inlet valve angle. The natural movement of the fluid is determined according to density difference based on Eq. (1) [15].

Table 1
Specifications of the understudied HTS transformer.

Parameters		Values
Power rating		120 kVA
Voltage (HV/LV)		6000 V/400 V
Operation frequency		50 Hz
HV winding	Winding type	Solenoid
	Radius (inner/outer)	274 mm/282 mm
	Height	172 mm
LV winding	Winding type	Double pancake
	Number of discs	13
	Radius (inner/outer)	220 mm/234 mm
	Height	172 mm
Operation temperature		77 K

Table 2
Specifications of HTS Transformer Cryostat.

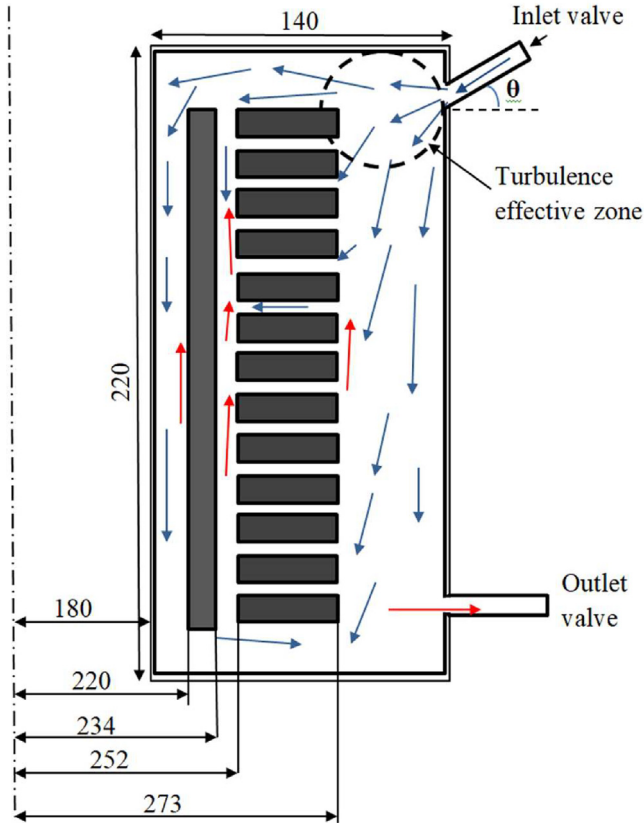| Cryostat parameters	Design values (mm)
Height	220
Inside/outside radius	180/320
Inlet/outlet pipe number	2
Inlet/outlet valve height	190/30
Inlet valve radius	10

Fig. 2. The path of LN$_2$ from the inlet valve to other parts of the cryostat and cryostat specifications (all the dimensions are reported in mm).

$$(\rho - \rho_0)g = -\rho_0\beta(T - T_0)g \tag{1}$$

where ρ and ρ_0 are liquid density at T and T_0 temperatures, respectively, and g is gravity and β is Tyndall's bar breaker.

The electromagnetic behavior of the HTS transformer is modeled based on Maxwell equation as presented in the following equations [23].

$$\nabla \times (\xi\nabla \times H) + \frac{\partial\mu_r H}{\partial t} = 0 \tag{2}$$

where H is the magnetic field intensity, ξ is charge density and μ_r is permeability.

The specific electrical resistance for superconducting windings is calculated by Eq. (3) [11]:

$$\sigma HTS = \frac{E_c}{J_c(B)}\left|\frac{J}{J_c(B)}\right|^{n-1} \tag{3}$$

where σHTS is the specific electrical resistance, J is the current density, $J_c(B)$ is the magnetic field dependant critical current density, and Eq. (4) shows the expression, E_c is the electric field criterion used to define the critical current and $n = 25$ is the index value in the E-J power law [24].

$$J_c(B) = \frac{J_{c0}}{\left(1 + \frac{\sqrt{\lambda^2 B_\parallel^2 + B_\perp^2}}{B_0}\right)^\gamma} \tag{4}$$

where, J_{C0} is the self-field critical current. $B_\parallel$ and $B_\perp$ are parallel and perpendicular components of magnetic field to the surface of HTS tapes.

The AC loss (in W/m) of the windings can be calculated by Eq. (5) [22].

$$Q_{AC} = f\int_0^{1/f}\int_s J.EdSdt \tag{5}$$

where, S and f are the cross section of superconducting tape and frequency of input current, respectively. E is the electric field.

Heat generation at top and bottom discs are higher than in central discs, due to higher magnetic fields in these parts. The heat generated in the windings is dissipated by a flow of LN$_2$. The main purpose of this paper is to increase LN$_2$ velocity and rate of turbulence to increase the rate of heat transfer. So, the determination of velocity and direction of LN$_2$ is critical. The conservation of mass equation, energy equation, and momentum equation to describe the motion of LN$_2$ are shown in Eqs. (6) to (8), respectively [25]:

$$\frac{\partial\rho}{\partial t} + \nabla.\rho\omega = 0 \tag{6}$$

$$\rho.\nabla\omega = F - \nabla P + u\nabla^2\omega \tag{7}$$

$$\rho c_p\omega.\nabla T = \nabla(k\nabla T) + q \tag{8}$$

where ρ is the density, ω is the fluid velocity, F is the force vector, u is the dynamic viscosity, P is the pressure, k is the thermal conductivity, T is the temperature, c_p is the specific heat of LN$_2$, and q is heat flux inside the transformer.

The main heat suppression method at the cryostat is heat convection. Eq. (9) is used to calculate the total transferred heat [26].

$$q_t = hA(T_s - T_f) \tag{9}$$

$$h = \frac{k}{l}Nu \tag{10}$$

In this equation, h is the convective heat-transfer coefficient, A is dimension of the cryostat, T_s is the temperature of windings, T_f is the LN$_2$ temperature, l is the characteristic length, $k = (1/3)C$th.vth. lth, is the thermal conductivity where Cth, vth and lth, respectively, are the specific heat, the velocity and the mean free path of thermal carriers [25], and Nu is the Nusselt number.

According to heat transfer theory, the Nusselt number in the turbulence state is calculated by Gnielinski's equation [27].

$$Nu = \frac{\left[\left(\frac{\mathcal{F}}{8}\right) \times (Re - 1000) \times \text{Pr}\right]}{\left[1 + 12.7 \times \left(\frac{\mathcal{F}}{8}\right)^{1/2} \times \left((\text{Pr})^{2/3} - 1\right)\right]} \tag{11}$$

where Re is the Reynolds Number, Pr is the Prandtl number and $\mathcal{F}$ is Darcy friction factor which calculated by Eq. (12) [27].

$$\frac{1}{\sqrt{\mathcal{F}}} = -2\log\left[\left(\frac{\left(\frac{\varepsilon_r}{d_i}\right)}{3.7}\right) + \left(\frac{2.51}{\left(\frac{Re}{\sqrt{\mathcal{F}}}\right)}\right)\right] \tag{12}$$

where, ε_r is the pipe's effective roughness thickness, D_h is the operating diameter of coils, μ is the dynamic viscosity and α is the thermal diffusion coefficient.

The Nusselt number of vertical plan and horizontal plan in laminar zone is shown in Eq. (13) and (14), respectively [28].

$$Nu_v = \left(0.825 + \frac{0.387Ra^{1/6}}{\left[1 + (0.492/Pr)^{9/16}\right]^{8/27}}\right)^2 \tag{13}$$

$$Nu_h = 0.27Ra^{\frac{1}{4}} \tag{14}$$

$$Pr = \frac{\omega}{\alpha} \tag{15}$$

$$Ra = \frac{g\psi(T_s - T_f)l^3\rho}{u\alpha} \tag{16}$$

where Pr is the Prandtl number, Ra is the Rayleigh number, α is the thermal diffusion coefficient, and Ψ is the expansion coefficient.

The k-epsilon model for turbulence is one of the common methods to simulate the mean flow characteristics for turbulent flow conditions. The turbulence transport equations in the k-epsilon model are shown in Eqs. (17) and (18) [29]:

- Turbulence energy transport:

$$\frac{\partial \rho k}{\partial t} + \frac{\partial}{\partial x_j}\left(\rho \omega_j \frac{\partial k}{\partial x_j} - \left(\mu + \frac{\mu_\tau}{\delta_k}\right)\frac{\partial k}{\partial x_j}\right) = \tau_{ij} S_{ij} - \rho\varepsilon + \varnothing_k \tag{17}$$

- Energy dissipation transport:

$$\frac{\partial \rho\varepsilon}{\partial t} + \frac{\partial}{\partial x_j}\left(\rho \omega_j \varepsilon - \left(\mu + \frac{\mu_\tau}{\delta_\varepsilon}\right)\frac{\partial \varepsilon}{\partial x_j}\right) = c_{\varepsilon1}\frac{\varepsilon}{k}\tau_{ij}S_{ij} - c_{\varepsilon2}f_2\rho\frac{\varepsilon^2}{k} + \varnothing_\varepsilon \tag{18}$$

$$f_2 = 1 - 0.3exp\left(-\left(\frac{\rho k^2}{\mu\varepsilon}\right)^2\right) \tag{19}$$

$$\varnothing_k = 2\mu\left(\frac{\partial\sqrt{k}}{\partial y}\right)^2 \ and \ \varnothing_\varepsilon = 2\mu\frac{\mu_t}{\rho}\left(\frac{\partial^2 u_s}{\partial y^2}\right)^2 \tag{20}$$

where ε is turbulent dissipation rate, k is the thermal conductivity, x_j is the space coordinate component; $j = 1,2,3$, ω_j is the mean flow velocity component in the x_j coordinate direction, μ is the molecular viscosity, S_{ij} mean strain rate tensor, τ_{ij} total stress tensor, μ_t is turbulent eddy viscosity, and constant parameters are $c_\mu = 0.09$, $c_{\varepsilon1} = 1.45$, $c_{\varepsilon2} = 1.92$, $\delta_k = 1.0$, $\delta_\varepsilon = 1.3$. In LN_2 at 77 K, the experimental diagram of Fig. 3 is used to calculate the Nusselt number by Reynolds number.

2.3. Perlator specification

Installing Perlator at the bottom of inlet valve will disrupt the coherence movement of LN_2 and will lead to increase in the turbulence. A circular Perlator with 5 mm radius which is installed in the inlet valve is shown in Fig. 4. To eliminate Eddy current, FRP materials are considered in the Perlator structure. The size of the Perlator is small compared to the cryostat and its weight is negligible. A small
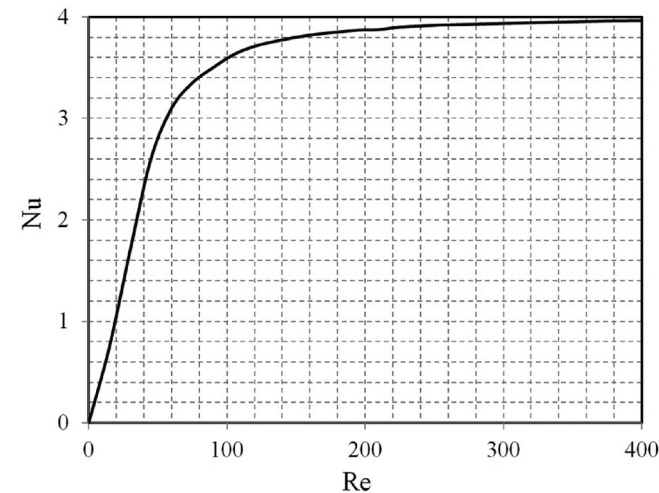

Fig. 3. Nusselt number diagram in terms of Reynolds number for LN_2 in 77 K [16].
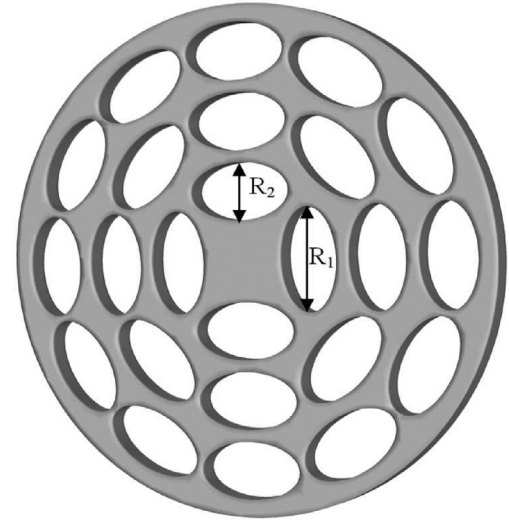

Fig. 4. Perlator structure.

Perlator made of fiberglass is the simplest and least expensive way to increase turbulence, and since it has no moving part, it will offer high reliability and a long life.

The porosity coefficient is a measure that is inversely related to fluid velocity reduction by the Perlator. Therefore, our purpose will be reaching the maximum value of the porosity coefficient. On the other hand, turbulence rate is directly related to the total perimeter of the cavities. The porosity of the Perlator is shown in Eq. (21):

$$\varphi = \frac{A_t}{A_p} \tag{21}$$

where A_t is the total area of the cavities and A_p is the area of the Perlator.

Increasing the effective perimeter of the inlet valve (by installing a Perlator) increases turbulence.

The Reynolds number, which indicates the intensity of the turbulence, is calculated from the following equations:

$$Re = \frac{\rho\omega D_H}{u} \tag{22}$$

$$D_H = \frac{4A_t}{P_t} \tag{23}$$

where ρ and u are the density and dynamic viscosity of LN_2, respectively. D_H is operating diameter and $\mathcal{V}$ is fluid velocity.

The equation of the total perimeter is as follows:

$$P_t = 2\pi N_h\sqrt{\frac{R_1^2 + R_2^2}{2}} \tag{24}$$

The total area of the cavities is based on the number of cavities layers.

$$A_t = N_h\pi R_1 R_2 \tag{25}$$

where P_t is the total perimeter of cavities, n is the number of rows of the cavities, $R_1 = \frac{4\pi R_p}{8N_h}$ is the big radius of elliptic, $R_2 = \frac{R_p}{2(N_h+1)}$ is the small radius of elliptic and r is the radius of Perlator.
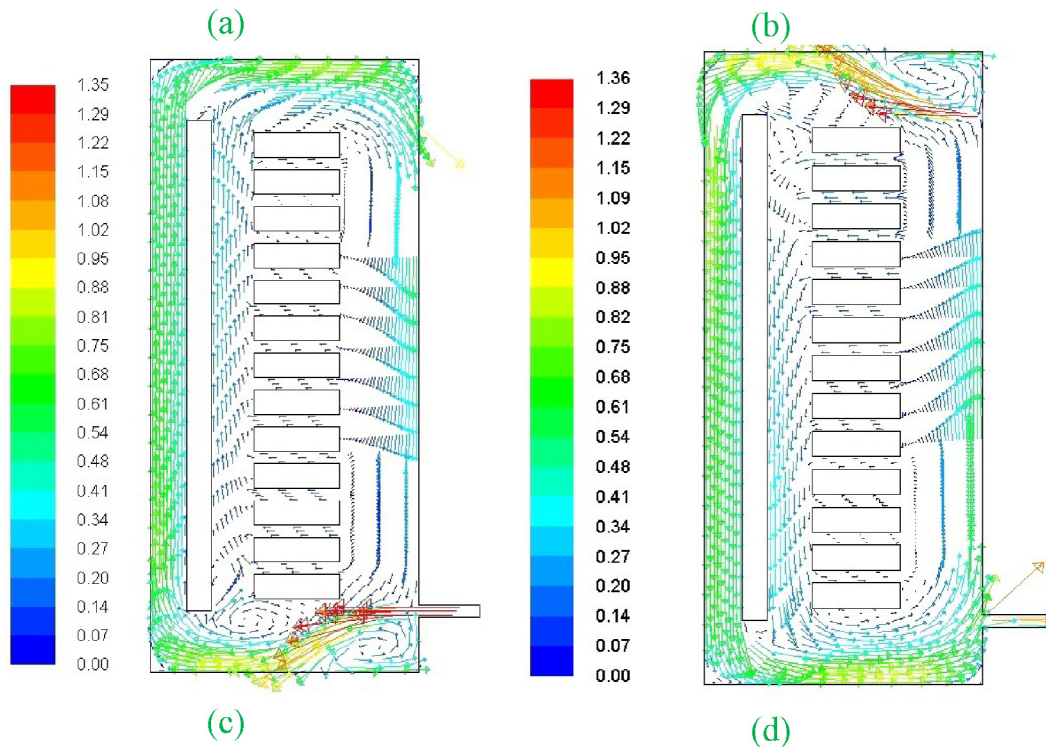
2.4. Cooling system operation

Eventually, LN_2 transfers heat into the cooling system and the temperature of LN_2 returns to 77 K. The heat generated while reducing LN_2 temperature to base temperature is determined by specific heat formula which shown in Eq. (26):
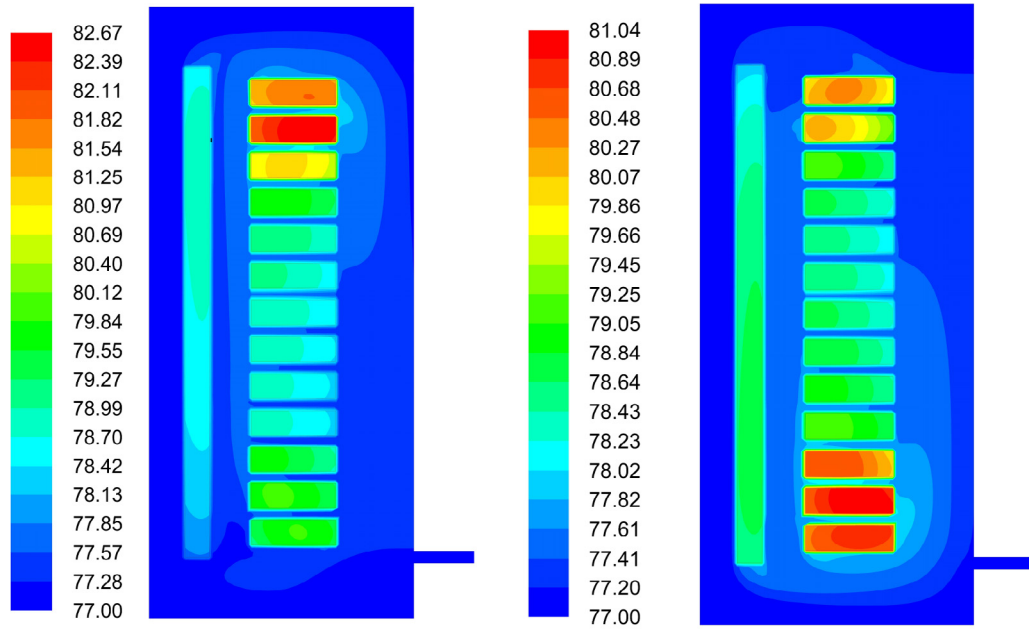
Contours of Static Temperature (k)

Contours of Static Temperature (k)

(a)

(b)

(c)

(d)

Fig. 5. Temperature distribution (K) and flow velocity (m/s) of the two different layouts of the inlet pipes. (a) and (c) Bottom inlet. (b) and (d) Top inlet.
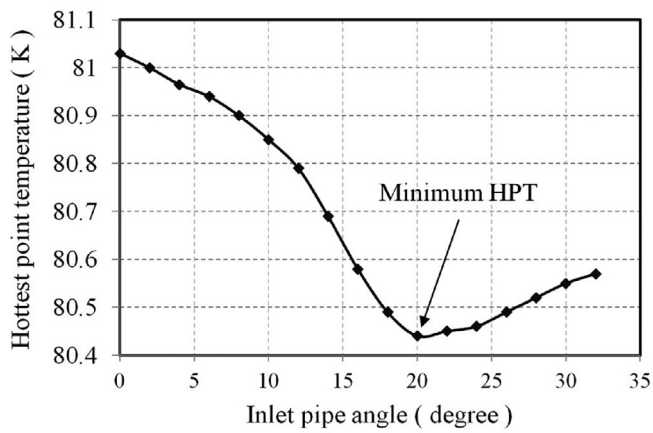
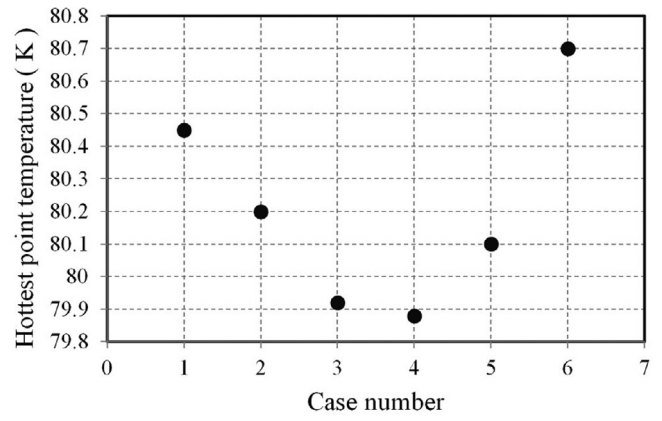**Fig. 6.** HPT comparison for different inlet valve angles.


Fig. 8. HPT changing by varying Reynolds number.

$$Q_c = mc(T_c - T_i) \tag{26}$$

where m is the mass, c is the specific heat capacity, T_c is the temperature of LN_2, $T_i = 77$ K is the base source temperature.

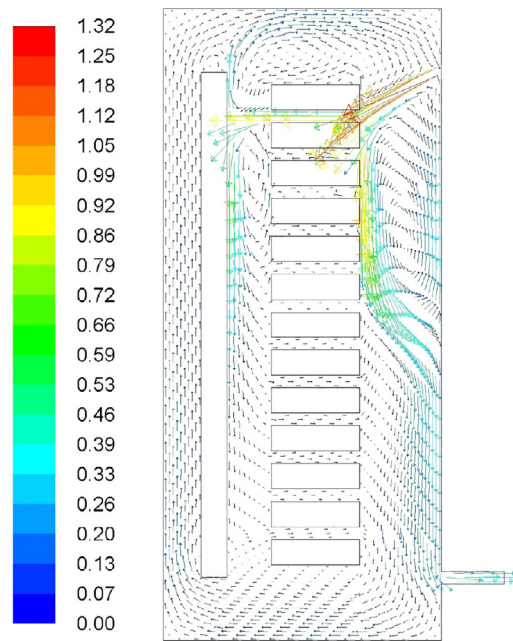The power of cooling system that absorbs Q_c at T_c and reject this at the room temperature can be expressed as [30]:

Table 4
specifications of the pipe and Perlator in Cryostat.

The details of inlet valve	Inlet pipe radius	10 mm
	Pipe angel	20°
Perlator	Number of tap hole	24
	R1/R2	2.3 mm/1.1 mm
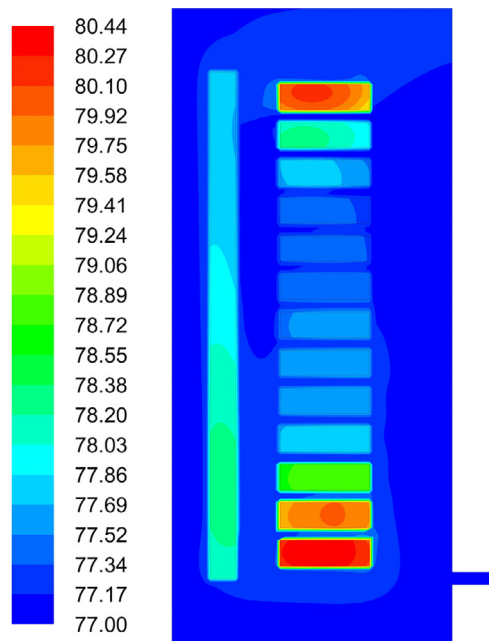
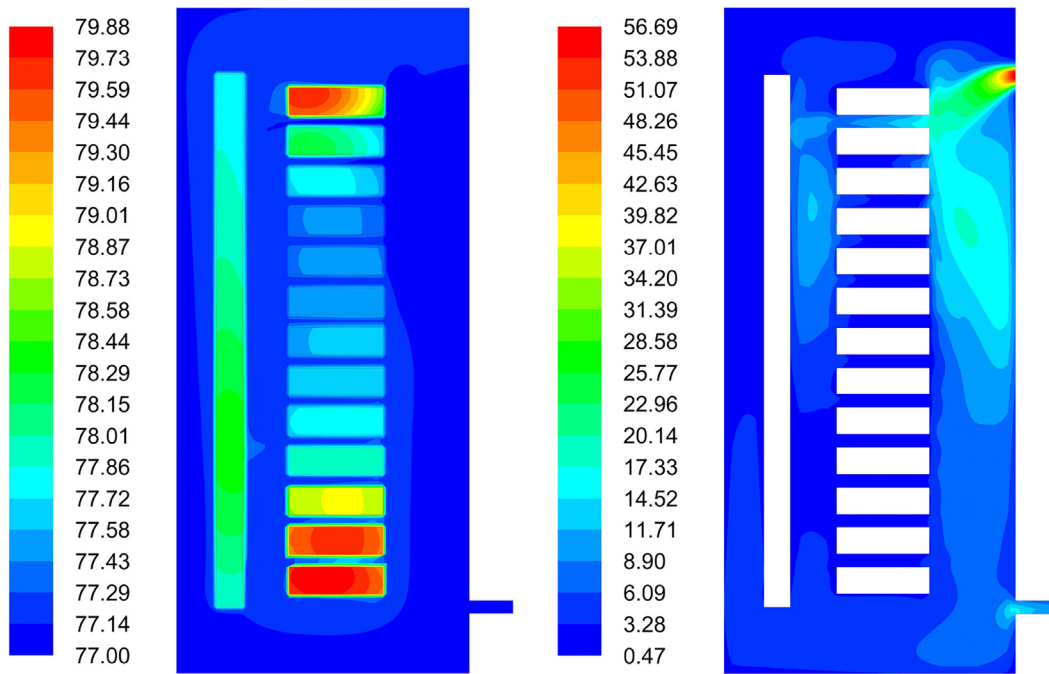Contours of Static Temperature (k)

(a)

Velocity Vectors Colored By Velocity Magnitude (m/s)

(b)

Fig. 7. (a) Temperature distribution (K) in $\theta = 20$ (b) flow velocity (in meters per second) of LN_2 in $\theta = 20$.

Table 3
Parameters of 6 case studies of the Perlator cavities.

Cavities Radius	Case 1	Case 2	Case 3	Case 4	Case 5	Case 6
R_1 (mm)	1.7	1.9	2.1	2.3	2.5	2.7
R_2 (mm)	1.7	1.5	1.3	1.1	0.9	0.7
N_h	21	21	24	24	24	24
R_1/R_2	1	1.2	1.6	2	2.7	3.8

Contours of Static Temperature (k)

(a)

Contours of Turbulent Intensity (%)

(b)
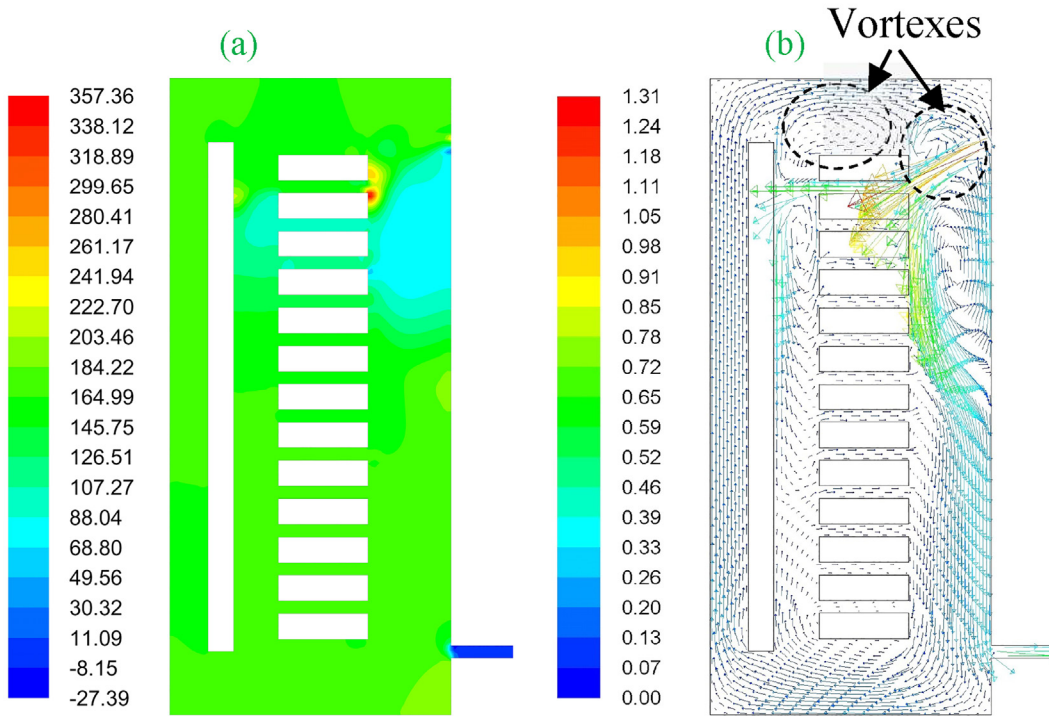
Contours of Static Pressure (pascal)

(c)

Velocity Vectors Colored By Velocity Magnitude (m/s)

(d)

Fig. 9. The optimum result after the Perlator placement (a) temperature distribution (b) turbulent intensity distribution (c) LN$_2$ pressure distribution (d) velocity vectors.

$$W = PNT \times Q_c \times \left(\frac{T_r}{T_c} - 1\right) \qquad (27)$$

where T_r is room temperature and PNT is Penalty factor of the cryocooler. We considered PNT value in 77 K as 15 in this study.

3. Results and discussions

The specifications of the understudied HTS transformer are given in [22]. Because of the high density of magnetic field in the top and bottom discs of double pancakes, AC loss in these discs is more than central discs. The calculation result shows that total AC loss in full load and non-optimized condition is 32.11 W and AC loss for HV and LV winding is 9.8 and 22.01 W, respectively [22]. Because of the natural LN_2 movement inside the cryostat, in the normal/rated condition, the temperature of the upper parts of the windings is more than the bottom parts. Therefore, it's reasonable that the inlet valve is placed on the upper side of the cryostat. The distribution of temperature and flow velocity in the two different layouts is shown in Fig. 5.

3.1. Inlet valve angle

Changing the inlet valve angle significantly affects the temperature of the bottom discs without increasing the temperature of the top discs. As shown in Fig. 5c the inlet LN_2 flow velocity mostly passes from the above of the top discs and it is directed with the natural movement of the LN_2. This phenomenon reduced the effect of LN_2 movement on the heat transfer. This case is optimized by changing the inlet valve angle. The HPT of the windings is calculated at different inlet pipe angles, as shown in Fig. 6. The lowest hottest point temperature is 81.04 which occurs at the inlet valve angle of 20°. Temperature distribution of windings and LN_2 in $\theta = 20$ is shown in Fig. 7a. Though the temperature of the top discs slightly increased, the hottest point temperature and temperature of the bottom discs decreased, significantly. The comparison between Fig. 5(d) and 7(b) shows that in $\theta = 20$, the path of cold LN_2 changes towards the walls of the top discs and reduces the temperature of these discs. In addition, a vortex forms near the upper discs, which helps to dissipate the heat generated by these discs. On the other hand, in $\theta = 20$ the collision between inlet LN_2 and natural movement of LN_2 in the turbulence effective zone (shown in Fig. 2), maximize the turbulence of the fluid.

3.2. Analysis of Perlator

Due to porosity rate, increasing the ratio R_1/R_2, in Perlator design would lead to an increase in turbulence and also inlet velocity reduction. The increase in the velocity and the turbulence of fluid, both lead to an increase in heat transfer.

On the basis of the radius of elliptic hole, specifications of the cavities are shown in Table 3. The HPT of winding for different cases in Table 3 was examined and the results are shown in Fig. 8.

As shown in Fig. 8, the lowest HPT point of winding occurs at case 4, and again increasing the R1/R2 in this structure increases the hottest point temperature of winding. Also, excessive increase of turbulence is lead to velocity reduction. As a result, HPT is increased which can cause a conversation in the fluid flow from the turbulence status to the linear status (See Table 4).

Fig. 9(a) shows the temperature distribution in the presence of the Perlator. As the results show, with adding Perlator, the temperature distribution in the double-pancakes become more uniform and the temperature of the discs has decreased. By adding Perlator, the HPT is reduced by 1.16 K compared to non-optimized condition.

Fig. 9(b) shows the fluid pressure distribution inside the cryostat. The pressure due to the increase in velocity and turbulence at the maximum state is about 0.357 kPa.

The force resulting from this amount of pressure is negligible against the strong electromagnetic Lorentz forces made by superconductors during their normal operation.

The AC loss is calculated for discs by Eq. (5). The result shows that total loss of LV winding for primary winding is 22.01 W but after reduction of temperature windings, the AC losses lease reduce to 20.42 W. The cooling power is reduced from 1297.77 to 1242.4 W based on Eq. (27). In the optimum state, the power of the cooling system is reduced by 4.26%.

4. Conclusion

In this study, a modified cryostat system for a 120 kVA, 6000/400 V High Temperature Superconducting (HTS) transformer is designed. Firstly, the angle of the inlet valve to reduce the winding temperature was examined and then the optimum inlet valve angle was obtained. Afterward, by designing a Perlator inside the inlet valve, the turbulence was increased, and it led to a significant reduction in winding temperature which eventually made a reduction in the AC losses. Heat analysis of winding temperature was done by ANSYS FLUENT software. The findings of this paper can be experimentally tested if an HTS transformer demonstrator is available.

Declaration of Competing Interest

The authors declare that they have no known competing financial interests or personal relationships that could have appeared to influence the work reported in this paper.

References

[1] Yamaguchi A, Nanato N, Obana T. Identification of normal transition in a bundle HTS cable used for an HTS transformer. Plasma Fusion Res 2021;16(4):2405065.

[2] Surdacki P, Woźniak Ł. Influence of the HTS winding tape on limiting the transient currents in superconducting transformers. Energies 2022;15(5):1688.

[3] Mohammad Yazdani-Asrami S, Gholamian A, Mirimani SM, Adabi J. Influence of field-dependent critical current on harmonic AC loss analysis in HTS coils for superconducting transformers supplying non-linear loads. Cryogenics 2021;113:103234.

[4] Wu Y, Song W, Wimbush SC, Fang J, Badcock RA, Long NJ, et al. Combined impact of asymmetric critical current and flux diverters on AC loss of a 6.5 MVA/25 kV HTS traction transformer. IEEE Trans Transp Electrif 2022.

[5] Liao X, Fang J, Zhao X, Song W, Yang S, Sun Y. Analysis of electromagnetic characteristics of 6.5 MVA/25 Kv HTS traction transformer using TA formulation. IEEE Trans Appl Supercond 2022.

[6] Song W, Jiang Z, Yazdani-Asrami M, Staines M, Badcock RA, Fang J. Role of flux diverters in reducing AC loss in a single-phase 6.5 MVA HTS traction transformer for Chinese high-speed train carrying high-order harmonic currents. IEEE Access 2022;10:69650–8.

[7] Fang X, Wang X, Sun Y, Song W, Pei X, Jiang Z, et al. Application of flux diverters in high temperature superconducting transformer windings for AC loss reduction. IEEE Trans Appl Supercond 2021;31(8):1–5.

[8] Mohammad Yazdani-Asrami M, Taghipour-Gorjikolaie WS, Zhang M, Chakraborty S, Yuan W. Artificial intelligence for superconducting transformers. Transform Mag 2021;8(S5):22–30.

[9] Staines M, Yazdani-Asrami M, Glasson N, Allpress N, Jolliffe L, Pardo E. Cooling systems for HTS transformers: impact of cost, overload, and fault current performance expectations. *Proc. 2nd Int. Workshop Cooling Syst. HTS Appl. (IWC-HTS)*, 2017.

[10] Majoros M, Jansak L, Zannella S, Curcio F, La Cascia P, Ottoboni V, et al. Temperature dependence of transport AC losses in Bi-2223/Ag multifilamentary tapes. Physica C 1998;310(1–4):6–11.

[11] Jiang Z et al. 15% reduction in AC loss of a 3-phase 1 MVA HTS transformer by exploiting asymmetric conductor critical current. J Phys Commun 2021;5 (2):025003.

[12] Liu G, Zhang G, Jing L, Hui Y. Numerical study on AC loss reduction of stacked HTS tapes by optimal design of flux diverter. Supercond Sci Technol 2017;30 (12):125014.

[13] Heydari H, Faghihi F, Aligholizadeh R. A new approach for AC loss reduction in HTS transformer using auxiliary windings, case study: 25 kA HTS current injection transformer. Supercond Sci Technol 2008;21(1):015009.

[14] Shen S, Tang Y, Ren L, Zuoshuai L, Chen W, Shi J. Design of cryogenic cooling system of a 35-kV/3.5-MVA single-phase HTS-controllable reactor. IEEE Trans Appl Supercond 2016;26(4):1–4.

[15] Kim SR, Han J, Kim WS, Park MJ, Lee SW, Choi KD. Design of the cryogenic system for 100 MVA HTS transformer. IEEE Trans Appl Supercond 2007;17(2):1935–8.

[16] Seungwhan B, Bradley PE, Radebaugh R. Heat transfer coefficient measurement of LN2 and GN2 in a microchannel at low Reynolds flow. Int J Heat Mass Transf 2018;127:222–33.

[17] Čarija Z, Franković B, Perčić M, Čavrak M. Heat transfer analysis of fin-and-tube heat exchangers with flat and louvered fin geometries. Int J Refrig 2014;45:160–7.

[18] Yazdani-Asrami M, Staines M, Sidorov G, Eicher A. Heat transfer and recovery performance enhancement of metal and superconducting tapes under high current pulses for improving fault current-limiting behavior of HTS transformers. Supercond Sci Technol 2020;33(9):095014.

[19] Prigozhin L. Analysis of critical-state problems in type-II superconductivity. Trans Appl Supercond 1997;7(4):3866–73.

[20] Zhang Y, Li J, Wang Z, Ren L, Guao S, Ying X, et al. Study on AC loss characteristics in HTS windings of a HTS controllable reactor with orthogonally configured core. IEEE Trans Appl Supercond 2019;29(5):1–5.

[21] Yazdani-Asrami M, Song W, Zhang M, Yuan W, Pei X. AC transport loss in superconductors carrying harmonic current with different phase angles for large-scale power components. IEEE Trans Appl Supercond 2020;31(1):1–5.

[22] Pi W, Wang T, Zhang H, Yang Y, Wang Y. Design and simulation of a 120 kVA single-phase HTS transformer. IEEE Trans Appl Supercond 2020;30(4):1–5.

[23] Brambilla R, Grilli F, Martini L. Development of an edge-element model for AC loss computation of high-temperature superconductors. Supercond Sci Technol 2006;20(1):16.

[24] Gömöry F, Vojenciak M, Pardo E, Šouc J. Magnetic flux penetration and AC loss in a composite superconducting wire with ferromagnetic parts. Supercond Sci Technol 2009;22(3):034017.

[25] Liao C, Ruan J, Liu C, Wen W, Zhiye D. 3-D coupled electromagnetic-fluid-thermal analysis of oil-immersed triangular wound core transformer. IEEE Trans Magn 2014;50(11):1–4.

[26] Bezaatpour M, Goharkhah M. Convective heat transfer enhancement in a double pipe mini heat exchanger by magnetic field induced swirling flow. Appl Therm Eng 2020;167:114801.

[27] Cengel Y, Ghajar A, Ma H. Heat and mass transfer fundamentals & applications. McGraw-Hill; 2015.

[28] Huang P, Bardina J, Coakley T. Turbulence modeling validation, testing, and development. NASA Technical Memorandum 1997;110446:10–2514.

[29] Wang Y. Fundamental elements of applied superconductivity in electrical engineering. John Wiley & Sons; 2013.

[30] Chang H-M, Choi YS, Van Sciver SW, Baldwin TL. Cryogenic cooling temperature of HTS transformers for compactness and efficiency. IEEE Trans Appl Supercond 2003;13(2):2298–301.